Journal of Hazardous Materials 427 (2022) 128156

Contents lists available at ScienceDirect

Journal of Hazardous Materials

journal homepage: www.elsevier.com/locate/jhazmat

Research Paper

Engineering linkage as functional moiety into irreversible thiourea-linked covalent organic framework for ultrafast adsorption of Hg(II)

Hai-Long Qian [a,b,d,*], Meng-Si Zhu [d], Mei-Lan Du [d], Xu-Qin Ran [d], Xiu-Ping Yan [a,c,d]

[a] State Key Laboratory of Food Science and Technology, Jiangnan University, Wuxi 214122, China
[b] Guangdong Laboratory for Lingnan Modern Agriculture, Guangzhou 510642, China
[c] Key Laboratory of Synthetic and Biological Colloids, Ministry of Education, School of Chemical and Material Engineering, Jiangnan University, Wuxi 214122, China
[d] Institute of Analytical Food Safety, School of Food Science and Technology, Jiangnan University, Wuxi 214122, China

HIGHLIGHTS

- Engineering COFs linkage as functional moiety to efficiently promote the adsorption kinetics for Hg(II).
- The first thiourea-linked COFs with high affinity to Hg(II).
- Thiourea-linked COFs with the rapidest adsorption kinetics for Hg(II) among all available adsorbents.

GRAPHICAL ABSTRACT

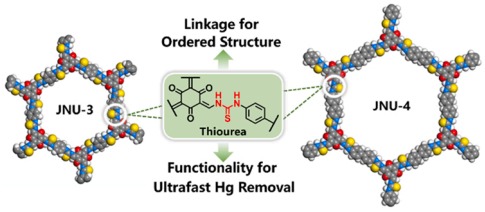

ARTICLE INFO

Editor: Dr. B. Sungjun

Keywords:
Thiourea-linked COFs
Irreversible COFs
Adsorbents
Ultrafast adsorption
Hg(II)

ABSTRACT

Development of novel functionalized covalent organic frameworks (COFs) as adsorbent for removal of mercury from environment is of great significance, but the conventional strategies for functionalizing COFs always sacrifice porous properties and suppress the exposure of functional sites, which goes against the rapid adsorption of Hg(II). Here, we show the rational design and preparation of the first thiourea-linked COFs via engineering the COFs linkage as functional moiety for ultrafast and selective adsorption of Hg(II). Two thiourea-linked COFs JNU-3 and JNU-4 were prepared via tautomerism reaction of 1,3,5-triformylphloroglucinol with 1,4-phenylenebis(thiourea) and 1,4-biphenylenebis(thiourea), respectively. The thiourea serves as not only linkage to connect the building block into irreversible crystalline structure, but also functional moiety to give no occupation of the COF pore and full exposure to Hg(II) with strong affinity, offering the JNU-3 and JNU-4 large adsorption capacity (960 and 561 mg g^{-1}, respectively) and ultrafast kinetics (equilibrium time of 10 s) for Hg(II). The proposed strategy for the design of functional COFs with inherent linkage as functional moiety largely promotes the performance of COFs for diverse applications.

1. Introduction

Mercury is growing as a huge threat to the ecological environment due to its high toxicity, bioaccumulation and persistence (Hsu-Kim et al., 2013; McNutt, 2013; Rahman and Singh, 2019). Development of efficient technologies for the removal of mercury in the environment is indispensable. Among the considerable methodologies, the application of functional adsorbent to capture mercury holds great potential (Albatrni et al., 2021; Huang et al., 2021; Huang and Shuai, 2019; Yu et al., 2016). Therefore, the exploration of novel adsorbents with rapid

* Corresponding author at: State Key Laboratory of Food Science and Technology, Jiangnan University, Wuxi 214122, China.
E-mail address: hlqian@jiangnan.edu.cn (H.-L. Qian).

https://doi.org/10.1016/j.jhazmat.2021.128156
Received 8 November 2021; Received in revised form 10 December 2021; Accepted 23 December 2021
Available online 28 December 2021

kinetics, high selectivity and large capacity for mercury is of great significance.

Covalent organic frameworks (COFs) as the superb representative of crystalline porous polymers show high potential as adsorbent, catalyst, sensor, and semiconductor owing to the combination of porosity with ordered periodic structure (Cui et al., 2021; Ding and Wang, 2013; Haase and Lotsch, 2020; Segura et al., 2016; Wu et al., 2019; Xu et al., 2015). The ordered structure of COFs with large surface areas allows the sufficient interaction of active sites with the target (Da et al., 2020). The diverse building monomers render COFs as a facile platform for functionalization to deeply influence their physicochemical properties including stability, host-guest interaction, and optical-electrical capability to meet the demands of diverse applications (Huang et al., 2016; Xu et al., 2021; Yusran et al., 2018). These unique properties make COFs promising as a efficient adsorbent for the removal of mercury.

To date, a few efforts have been made to prepare functionalized COFs as adsorbent for the removal of mercury (Cui et al., 2020; Ding et al., 2016; Huang et al., 2017; Merí-Bofí et al., 2017; Sun et al., 2017; Zhang et al., 2021). Ding et al. prepared a (ethylthio)propoxy functionalized COF (COF-LZU8) via bottom-up approach for simultaneous detection and capture of Hg(II). The concentration of Hg(II) evidently decreased from 10 to 0.2 mg L^{-1} after adsorption with COF-LZU8 for 3 h (Ding et al., 2016). Additionally, another sulfur-based COF (COF-S-SH) was also synthesized through the post-synthetic thiol-ene click reaction of vinyl-functionalized COF (COF-V) and 1,2-ethanedithiol for efficient adsorption of Hg(II) with equilibrium time of 10 min (Sun et al., 2017). However, all the functionalized COFs for Hg(II) were prepared via bottom-up or post-synthetic method to anchor the functional groups into the pores of COFs. The steric hindrance of the functional groups always leads to the damage of the porous structure of COFs including crystallinity, surface area, and pore volume to a certain extent. Moreover, the functional chain entanglement results in the shielding of active sites. These functionalization-induced damages of porous structure and shield of active sites in COFs go against rapid diffusion and kinetics of functionalized COFs for the adsorption of analytes (Huang et al., 2017; Karak et al., 2019). Although Huang et al. introduced a short sulfide chain to promote the adsorption of Hg(II) on the functionalized COF (Huang et al., 2017), more efficient strategies are still imperative. As the connection of building units, the linkage shows uniform distribution and no occupation on the pore in COFs. Therefore, engineering the COFs linkage as functional moiety is an efficient strategy to avoid the above-mentioned negative effects of conventional functionalization on the adsorption of Hg(II) with COFs, but has not been explored so far.

Herein, we report an efficient strategy for rational design of functionalized COFs via engineering the COFs linkage as functional moiety to promote the adsorption kinetics of Hg(II) with COFs. The special dithizone structure with both sulfur and nitrogen makes thiourea good affinity for mercury (Jiang et al., 2012). We take thiourea as proof-of-concept to design and prepare the first irreversible thiourea-linked COFs for ultrafast and selective adsorption of Hg(II). Thiourea is employed not only to serve as the linkage but also the functional moiety to preclude the negative effects of conventional functionalization on the pore as well as the shield of active sites, endowing the COFs ultrafast and selective adsorption of Hg(II). The developed strategy for the design of irreversible COFs with the linkage as the functional moiety has great potential for diverse applications.

2. Experimental methods

2.1. Preparation of 1,4-phenylenebis(thiourea)

1.078 g of ammonium thiocyanate (Atc) in 10 mL H_2O was dropwise added to 170 mg p-phenylenediamine (Pa) at 0 °C. After further addition of 600 μL concentrated HCl, the reaction mixture was stirred at 0 °C for 30 min, and then reacted at 90 °C for 15 h. The mixture was filtrated to collect the product after cooling to room temperature. The obtained product was washed with water and dried at 80 °C for 12 h under reduced pressure to obtain the 1,4-phenylenebis(thiourea) (Pa-S) in 86.2% yield. 1H NMR (400 MHz, DMSO-d6) δ 9.65 (s, 2H), 7.33 (s, 4H); 13 C NMR (100 MHz, DMSO-d6) δ 181.46, 135.98, 124.22. *m/z* (ESI-MS) 225.02, $[M\text{-}H]^-$ (calcd. 225.03).

2.2. Synthesis of JNU-3

A mixture containing 1,3,5-triformylphloroglucinol (Tp, 21.0 mg, 0.1 mmol), Pa-S (33.9 mg, 0.15 mmol), N,N-dimethylacetamide (DMAC, 0.8 mL), and 1,2-dichlorobenzene (o-DCB, 0.2 mL) were sonicated in a 35-mL Schlenk tube (OD 26 × L 125 mm) for 5 min. After addition of 12 M Acetic acid (HAc, 0.1 mL), the solution was further sonicated for 15 min and degassed with freeze–pump–thaw cycles. Then, the tube was sealed and left undisturbed at 60 °C for 3 days. The resulting red precipitate was collected via centrifugation and rinsed with N,N-dimethylformamide. The crude product was extracted with methanol and vacuum-dried at room temperature for 5 h to obtain JNU-3 (yield, ca.72.6%).

2.3. Adsorption experiment

Typically, 5 mg JNU-3 was mixed with 5 mL of 100 mg L^{-1} Hg(II). After adsorption equilibrium, the JNU-3 was isolated with 0.22 μm syringe-driven filter. The filtrate was collected for inductively coupled plasma mass (ICP-MS) determination of Hg.

2.4. Effect of pH on adsorption

5 mg JNU-3 was mixed with 5 mL of 400 mg L^{-1} Hg(II) solution at different pH (1–7) till equilibrium. The mixture was treated with 0.22 μm syringe-driven filter, and the filtrate was collected for ICP-MS determination of Hg.

2.5. Effect of time on adsorption

5 mg JNU-3 was mixed with 5 mL of 10 mg L^{-1} Hg(II) solution at pH 4 for a predetermined time (10–10800 s). The mixture was treated with 0.22 μm syringe-driven filter, and the filtrate was collected for ICP-MS determination of Hg.

2.6. Quantum mechanics calculation

The density functional theory (DFT) calculation with B3LYP function and 6–31 G/Def2SVP basis set on Gaussian 09 was performed to elucidate the interaction of JNU-3 and Hg(II). One-unit cell of JNU-3 was used as the model structure to evaluate the adsorption energy (E_{ad}) on the basis of following equation:

$$E_{ad} = E_{JNU\text{-}3\text{-}Hg} - (E_{JNU\text{-}3} + E_{Hg})$$

where $E_{JNU\text{-}3\text{-}Hg}$, $E_{JNU\text{-}3}$ and E_{Hg} represent the energy of the JNU-3 adsorbed with Hg(II), isolated JNU-3 and Hg(II) after geometry optimization, respectively.

3. Results and discussion

3.1. Design and preparation of thiourea-linked COFs

The rapid mass transfer and kinetics of porous materials largely depend on the accessibility of extensively open pore (Karak et al., 2019). Although the functionalization of the ordered structure endows COFs great potential for removal of Hg(II), the conventional strategies for introducing desirable functionality to COFs by anchoring the functional groups in their pore usually impair the porosity, crystallinity, surface area of COFs along with the shield of active sites, leading to the decrease

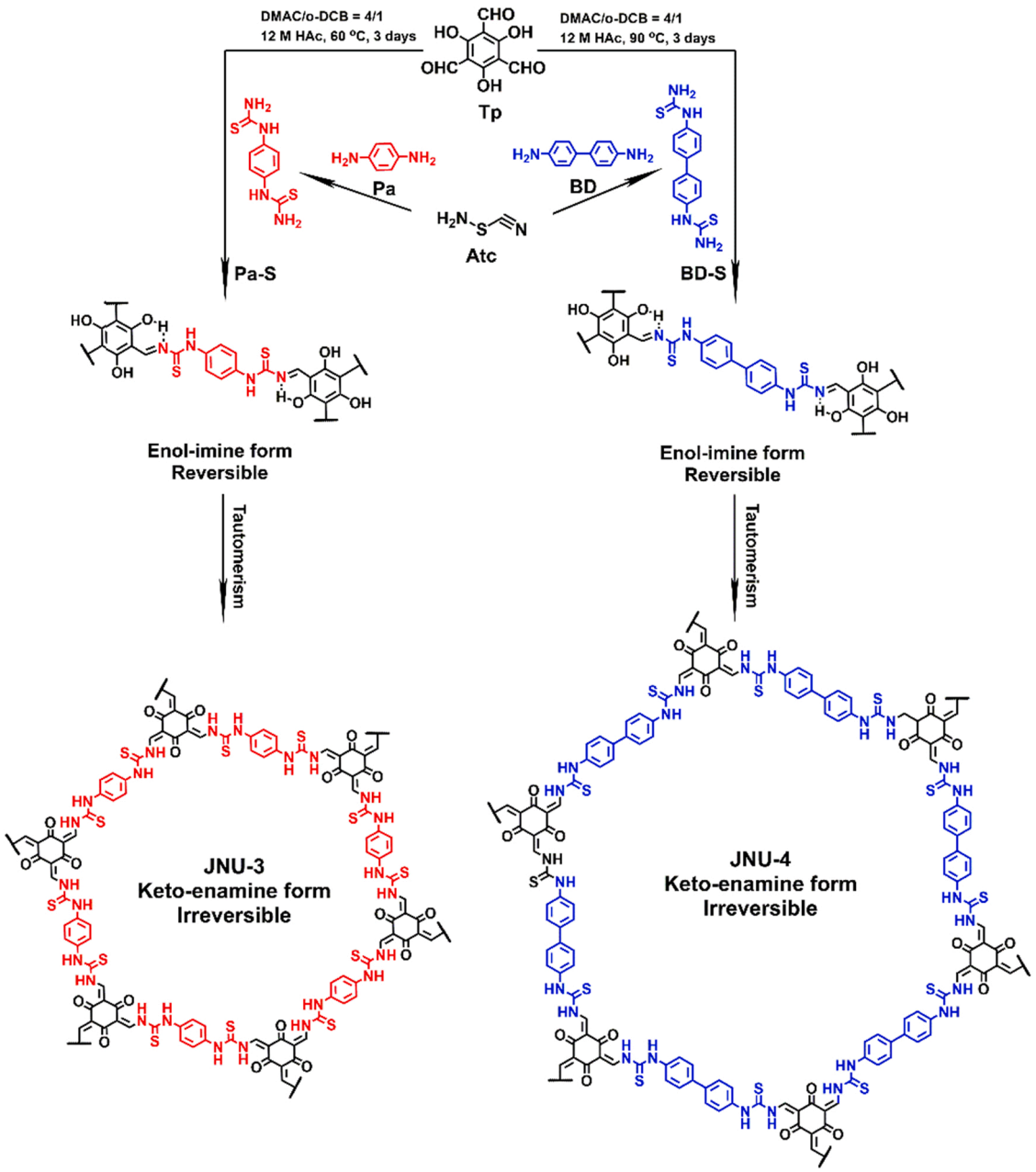

Fig. 1. Design of tautomerism reaction for the synthesis of thiourea-linked COFs JNU-3 and JNU-4 with Tp, Pa-S and BD-S as precursors.

of the adsorption kinetics of Hg(II). The engineering linkage as the functional moiety is a promising strategy to eliminate the above-mentioned negative influences resulting from conventional functionalization.

Fig. 1 shows such a strategy for the design of irreversible thiourea-linked COFs with thiourea as both the linkage and the functional group for the adsorption of Hg(II). The amino precursors Pa-S and 1,4-biphenylenebis(thiourea) (BD-S) were first synthesized by reacting Atc with Pa and benzidine (BD), respectively (Fig. 1 and S1-S8). Tp was selected as the aldehyde monomer to condense with Pa-S and BD-S due to the special tautomerization reaction (Chong et al., 2003; Kandambeth et al., 2012). The formed reversible enol-imine was transferred to irreversible keto-imine structure to give thiourea-linked COFs JNU-3 and JNU-4 with original crystallinity and improved stability (Fig. 1). The irreversible thiourea not only linked the organic unit to form highly stable structure, but also served as inherent functionality due to its affinity to Hg(II). The developed unique strategy for the functionalization of COFs gives almost no occupation of pore and shield of active sites to take full advantage of the complete pore of COFs for ultrafast adsorption of Hg(II).

Regulation of solvent, temperature, and time for the condensation of the precursors is important for facilitating the formation of ordered crystalline structure of COFs (Fig. S9-S14). Crystalline JNU-3 was synthesized via the condensation of Tp and Pa-S with DMAC/o-DCB (4/1, v/v) and 12 M acetic acid (HAc) as solvent at 60 °C for 3 days, while JNU-4 was obtained with the reaction of Tp and BD-S under the condition of DMAC/o-DCB (4/1, v/v) and 12 M HAc at 90 °C for 3 days.

3.2. Characterization of thiourea-Linked COFs

Powder X-ray diffraction (PXRD) in combination with computational simulation is a common structural resolution for COFs (Ding and Wang, 2013). The rotational thiourea bond might give various conformations of the prepared thiourea-linked COFs in analogy to urea-linked COFs

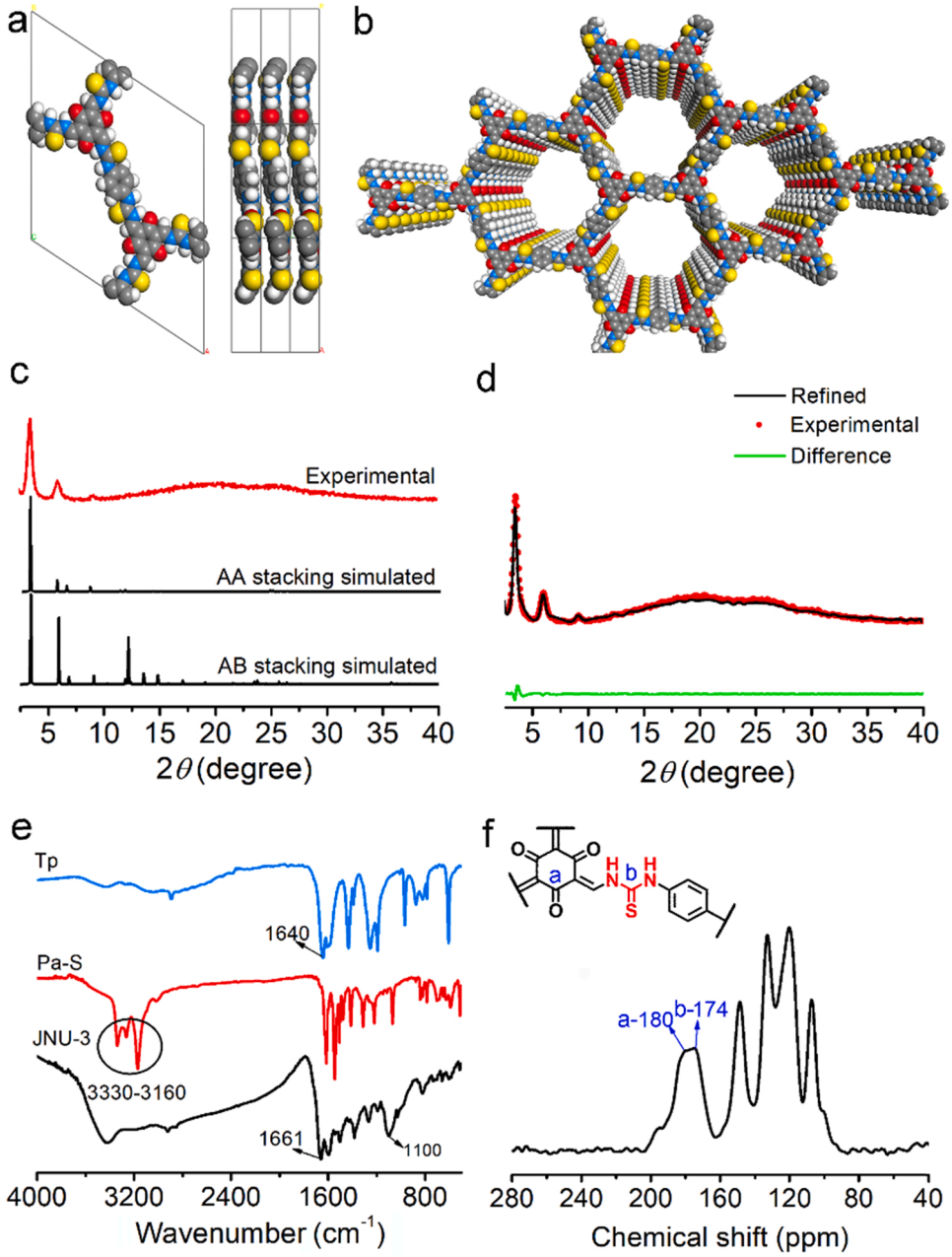

Fig. 2. (a) Unit cell of JNU-3 in AA stacking model. (b) Space-filling model of JNU-3 in AA stacking model (gray C, sky-blue N, red O, yellow S, white H). (c) Experimental and simulated (AA and AB stacking model) PXRD patterns of JNU-3. (d) Pawley refinement of JNU-3 (Rwp = 5.71%, Rp = 3.65%). (e) FTIR spectra of Tp, Pa-S and JNU-3. (f) ^{13}C SNMR spectra of JNU-3.

(Zhao et al., 2018). The geometrical energy optimization with Forcite calculation can be applied to confirm the highest feasibility of COFs conformation (Ma et al., 2016; Wu et al., 2018; Zhu et al., 2015). Six possible 2D structures of JNU-3 with similar simulated PXRD pattern were generated and optimized with Forcite module (Fig. S15). Conformation A with unit cell parameters (a = b = 30.7947 Å, c = 3.7766 Å) at P-3 gave the most negative total energy (− 341.3 kcal mol^{-1}) than the other five conformations B-F (− 303.1 to − 224.9 kcal mol^{-1}), and thus is the most favorable conformation for JNU-3. Further structural resolution of JNU-3 based on Conformation A showed that the experimental PXRD pattern with several obvious diffraction peaks at 3.50°, 5.99° and 9.05° agreed well with that of AA stacking model rather than AB stacking (Fig. 2a–c and S16). Pawley refinement gave more precise unit-cell with a = b = 29.7273 Å, c = 3.7843 Å and α = β = 90°, γ = 120° (R_{wp} = 5.71%, R_p = 3.65%) (Table S1 and Fig. 2d).

The thiourea linkage was confirmed by Fourier transform infrared (FTIR) spectrometry. The simultaneous absence of characteristic -NH_2 (3330–3160 cm^{-1}) and -CHO (1640 cm^{-1}) peaks in the FTIR spectra of JNU-3 indicates the complete condensation of the amine and aldehyde precursors (Fig. 2e). The evident new FTIR peaks at 1661 and 1110 cm^{-1} were assigned to the stretching bands of C═O and C═S, indicating the formation of ketone and thiourea in the frameworks, respectively. An obvious peak at 180 ppm in ^{13}C solid-state nuclear magnetic resonance (SNMR) spectra of JNU-3, resulted from the carbon signal of ketone (C═O), further confirmed the new formation of keto-form structure. The thiourea carbon (C═S) peak at 174 ppm indicates the formation of thiourea linkage as well (Fig. 2f and S17).

The BET surface area, the pore size, pore volume of JNU-3 calculated from the nitrogen adsorption isotherm were 420 m^2 g^{-1}, ca. 16 Å and 0.77 cm^3 g^{-1}, respectively (Fig. S18 and S19). The porous structure of

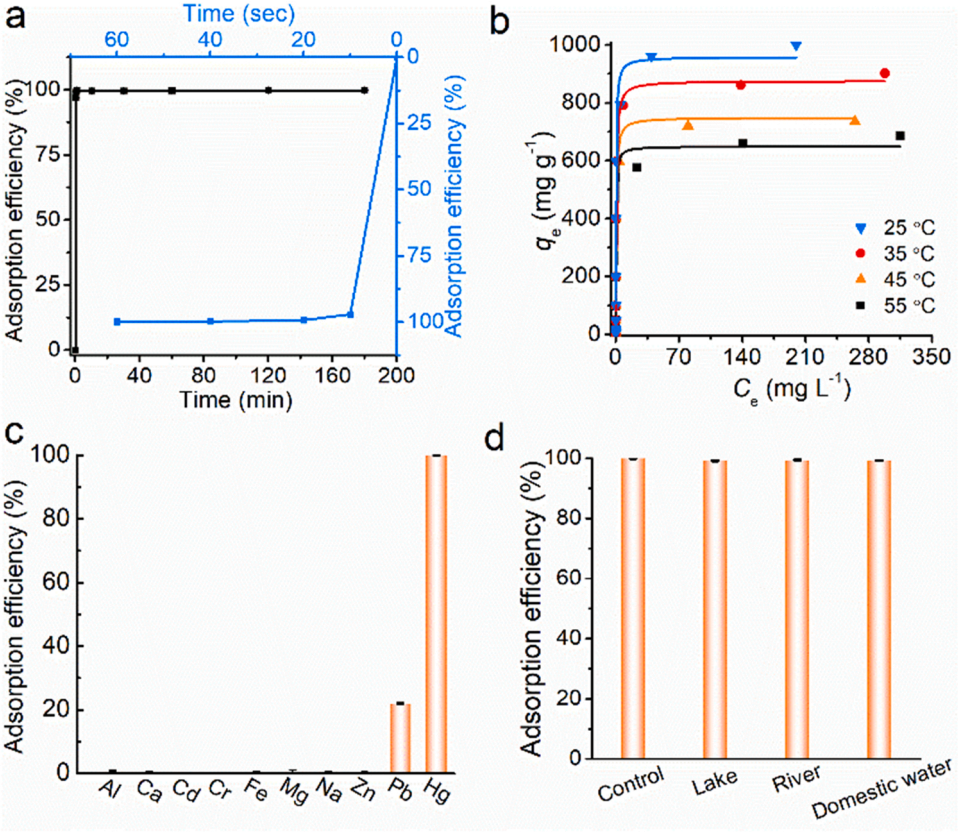

Fig. 3. (a) Time-dependent adsorption of Hg(II) on JNU-3. (b) Adsorption isotherms of Hg(II) on JNU-3 in the initial concentration range of 5–1200 mg L^{-1} at a predetermined temperature (25–55 °C). (c) Adsorption efficiency of metal ions on JNU-3 with the initial mixed metal ion concentration of 10 mg L^{-1}. (d) Adsorption of Hg(II) on JNU-3 from the river, lake, and domestic water samples with spiked Hg(II) concentration of 10 mg L^{-1}.

JNU-3 was also confirmed by scanning electron microscopy (Fig. S20). JUN-3 maintained the crystallinity in various solutions (Fig. S21), indicating its high chemical stability. The high surface area of JNU-3 with microporous and stable structure makes it high potential in further application.

Another thiourea-linked COF JNU-4 prepared by the condensation of Tp and BD-S gave an experimental PXRD pattern with three peaks at 2.86°, 4.90° and 7.30°, matching well with the simulated pattern from the refined AA stacking unit-cell (a = b = 38.0609 Å, c = 3.7331 Å and α = β = 90°, γ = 120°) with R_{wp} 2.89% and R_p 1.51% (Table S2, Fig. S22-S25). The evident FTIR peaks at 1662 and 1118 cm^{-1} and ^{13}C SNMR peaks at 180 and 174 ppm verified the formation of thiourea and ketone (Fig. S26 and S27). JNU-4 gave the BET surface of 1050 m^2 g^{-1}, pore size of ca. 34 Å and pore volume of 3.0 cm^3 g^{-1} (Fig. S18-S19) with obvious porous structure (Fig. S20) and high chemical stability (Fig. S28).

3.3. Adsorption of Hg(II)

We further systematically investigated the adsorption ability of JNU-3 for Hg(II). The effect of pH on the adsorption efficiency of Hg(II) with JNU-3 was studied in the pH range of 1–7 due to the formation of insoluble $Hg(OH)_2$ at higher pH. The pH exhibited little influence on the adsorption. JNU-3 can capture almost all the Hg(II) at pH 1–7 (Fig. S29). The pH 4 gave the best adsorption efficiency (99.7%), and was chosen for further experiments.

The adsorption kinetics plays a crucial role for the development of efficient adsorbents. The capture of Hg(II) on JNU-3 reached equilibrium within about 10 s, which is the shortest equilibrium time (t) for the adsorption of Hg(II) among the reported adsorbents (Fig. 3a). The concentration of Hg(II) sharply decreased from 10 mg L^{-1} to 0.002 mg L^{-1} in 10 s. After two-run adsorption, the concentration of Hg (II) was lower than the emission standards of drinking water (0.001 mg L^{-1}). JNU-3 gave a 10–100 times faster adsorption of Hg(II) than the COFs with functional moiety in the pore including COF-S-SH, TAPB-BMTTPA-COF and JUC-570, indicating the excellent availability of a specific group as both the linkage and the functionality to promote adsorption kinetics (Table S3). The pseudo-second-order mode (R^2 = 0.9999) fitted better with the adsorption kinetics than the pseudo-first-order model (R^2 = 0.9585), indicating the involvement of chemisorption (Table S4) (Qian et al., 2020). The pseudo-second-order rate constants K_2 was calculated to be 51.2 g mg^{-1} min^{-1}. The applicability of the pseudo-second-order model implies the adsorption rate was controlled by intraparticle diffusion (Plazinski et al., 2013), and further demonstrates that the ultrafast kinetics of JNU-3 resulted from the ordered structure and no occupation of the pore.

The adsorption performance of JNU-3 was further evaluated with the adsorption isotherms and distribution coefficient (K_d). The adsorbed Hg (II) on JNU-3 increased significantly at low initial concentration of Hg (II), then trended to be unchanged with further increase of the initial concentration (Fig. 3b). Three adsorption models (Langmuir, Freundlich and Temkin) were used to fit the adsorption isotherms of Hg(II) on JNU-3 (Cui et al., 2019; Linwei et al., 2019; Zou et al., 2016). The Langmuir model was best fitted to the adsorption isotherms among the three models (Fig. S30). The maximum adsorption capacity (q_m) of JNU-3 for Hg(II) was calculated to be 959 mg g^{-1}, comparable to those of most adsorbents (Table S3). The K_d of JNU-3 for Hg(II) was calculated to be 1.42 × 10^6 mL g^{-1}, indicating its strong affinity to Hg(II) (Fryxell et al., 2005).

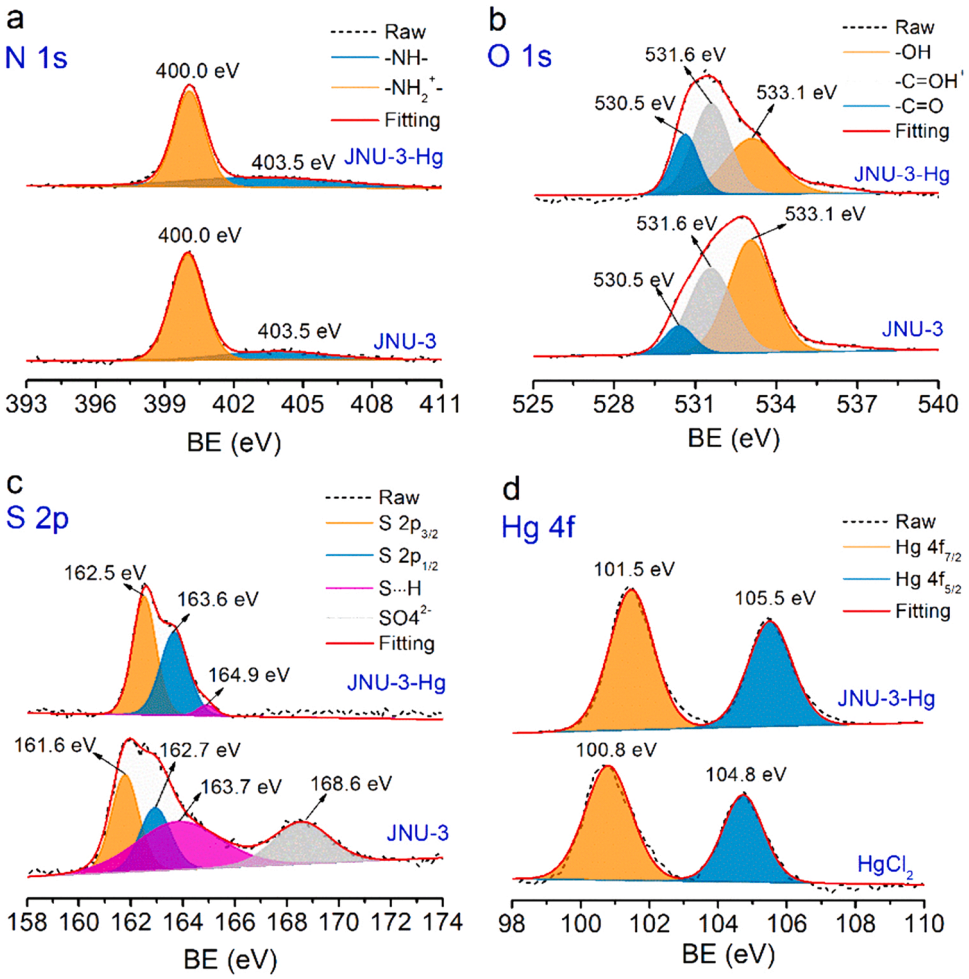

Fig. 4. XPS spectra of N 1s (a), O 1s (b) and S 2p (c) of JNU-3 and JNU-3-Hg. (d) XPS spectra of Hg before and after adsorption on JNU-3.

3.4. Selectivity

Selectivity is another important capability of adsorbents. JNU-3 still effectively adsorbed almost all Hg(II) (99.9%), but negligible competitive ions of Al^{3+}, Ca^{2+}, Cd^{2+}, Cr^{3+}, Fe^{3+}, Mg^{2+}, Na^{+}, Zn^{2+}, and Pb^{2+} (Fig. 3c) due to the significantly higher complexation constant of the sulfur in JNU-3 for Hg(II) than other ions (Merrifield et al., 2004; Pearson, 1968). The result shows the high selectivity of JNU-3 for Hg(II). The practical capacity of JNU-3 was assessed by using lake, river and domestic water to prepare samples. The slight change of the adsorption efficiency (99.4–99.1) with the initial Hg(II) concentration of 10 mg L^{-1} suggested the potential of JNU-3 for the removal of Hg(II) in real sample (Fig. 3d).

3.5. Cycle adsorption performance

The cycle performance is also a critical performance parameter for an adsorbent. The Hg(II) can be desorbed from the JNU-3 with the eluent containing 1 mol L^{-1} thiourea and 1 mol L^{-1} HCl. JNU-3 still gave 94.0% of adsorption efficiency for Hg(II) after 4 run adsorption-desorption process (Fig. S31). The unchanged FTIR spectra reveal the adsorption of Hg(II) exhibited no obvious negative effect on the JNU-3 structure (Fig. S32). The PXRD pattern of regenerated JNU-3 indicates the decrease of crystallinity after the adsorption of Hg(II) (Fig. S33).

3.6. Adsorption mechanism

To get an insight into the mechanism for the adsorption of Hg(II) on JNU-3, the thermodynamics of the adsorption was first investigated. The negative free energy change (ΔG) and enthalpy change (ΔH) indicate the spontaneity and exothermicity of the adsorption, respectively. Furthermore, the adsorption was driven by both enthalpy and entropy due to $\Delta H < 0$ and entropy change (ΔS) > 0 (Fig. S34 and Table S5). To Figure out the active sites of JNU-3 for the adsorption of Hg(II), TpPa-1, having similar structure of JNU-3 but containing no thiourea was prepared for comparison (Fig. S35). TaPa-1 gave much lower adsorption capacity (148 mg g^{-1}) than JNU-3 (959 mg g^{-1}), demonstrating the dominant role of thiourea in the adsorption.

X-ray photoelectron spectroscopy (XPS) was applied to further verify the roles of N, O, S in JNU-3 in the adsorption of Hg(II). Wide XPS scanning spectra of Hg(II) adsorbed JNU-3 (JNU-3-Hg) gave two evident peaks of Hg $4f_{7/2}$ and Hg $4f_{5/2}$, confirming the capture of Hg(II) on JNU-3 (Fig. S36). The same N 1s XPS spectra of JNU-3 and JNU-3-Hg implies no involvement of N in the adsorption (Fig. 4a). Although the unchanged position of three fitted peaks in O 1s XPS spectra verified the O also did not coordinate with Hg, the obvious reduction of peak area at 533.1 eV indicates the decrease of adsorbed -OH on JNU-3 after the adsorption of Hg(II) (Fig. 4b). The S 2p XPS spectra of JNU-3 was fitted into four peaks at 161.6, 162.7, 168.6 and 164.9 eV, assigned to the S $2p_{3/2}$, S $2p_{1/2}$, the hydrogen bond interacted S (S···H), and the adsorbed SO_4^{2-} (Huang et al., 2020, 2017). After the adsorption of Hg(II), the adsorbed SO_4^{2-} was rinsed. The S 2p3/2 and S 2p1/2 peaks shifted from 161.6 and 162.7 eV to 162.5 and 163.6 eV, respectively. The almost disappearance of peak for the S···H demonstrates most of S are interacted with Hg(II) (Fig. 4c). Moreover, the Hg XPS of JNU-3-Hg also displayed 0.7 eV shift compared with that of $HgCl_2$ (Fig. 4d), further confirming the

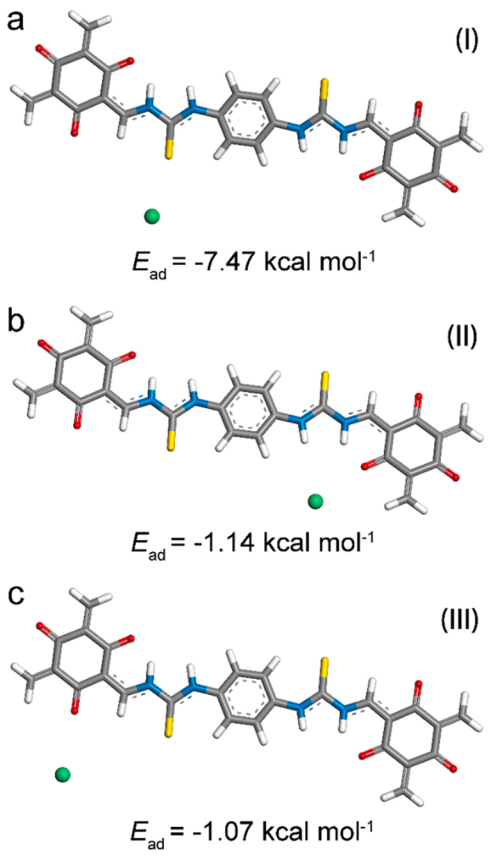

Fig. 5. Representative configurations and the corresponding E_{ad} of JNU-3-Hg obtained from quantum mechanics calculation (gray, C; blue, N; yellow, S; red, O; white, H; green, Hg).

interaction of S and Hg.

The configuration of JNU-3-Hg was revealed through quantum mechanics calculation. On the basis of JNU-3 structure, three configurations (I, II, III) of JNU-3-Hg were built with the possible binding sites of C═S, N-H and C═O, respectively (Fig. 5). After the geometry optimization with Gaussian 09 package (Frisch et al., 2013; Yoo et al., 2016), Configuration I, II, and III gave the E_{ad} of − 7.47, − 1.14 and − 1.07 kcal mol^{-1}, respectively. The most negative E_{ad} of Configuration I indicates the sulfur of thiourea is the most feasible binding sites of JNU-3 for Hg(II).

Furthermore, the adsorption performance of Hg(II) on JNU-4 was also studied. Similarly, JNU-4 showed the ultrafast adsorption kinetics to the Hg(II) with equilibrium time of 10 s (Fig. S37), indicating the universality of the proposed strategy in promoting adsorption kinetics. The adsorption kinetics and isotherms of Hg(II) on JNU-4 were fitted well with the pseudo-second-order and Langmuir model, respectively (Table S6 and Fig. S38). The JNU-4 gave a q_m of 561 mg g^{-1} for Hg(II) with strong affinity (K_d, 1.69×10^6 mL g^{-1}) and good selectivity (Fig. S39 and S40). The same weight of JNU-3 contains more content of thiourea than JNU-4 to interact with the Hg(II) due to the larger relative molecular mass of BD-S than Pa-S, leading to the higher capacity of JNU-3 for Hg(II) than the JNU-4.

4. Conclusion

In summary, we have reported an efficient strategy for the rational design of functionalized COFs with a specific group as both the linkage and the functional moiety to promote the adsorption kinetics with COFs. In the proof-of-concept, the first irreversible thiourea-linked COFs JUN-3 and JNU-4 were prepared for ultrafast and selective adsorption of Hg (II). The thiourea formed by the tautomerism reaction of Tp and dithiourea monomers not only acts as the linkage of the organic units to form irreversible crystalline JNU-3 and JNU-4 with high stability and large BET surface area, but also serves as the specific functional group for the adsorption of Hg(II). The employment of thiourea linkage as functional moiety allows the no occupation of pore and the maximal exposure of functionality, offering thiourea-linked COFs the highest kinetics to Hg(II). This work provides a unique strategy for the functionalization of COFs without additional occupation of pore and shield of active sites to take full advantage of the complete pore of COFs for diverse applications.

CRediT authorship contribution statement

Hai-Long Qian: Conceptualization, Methodology, Writing – original draft, Writing – review & editing, Supervision, Funding acquisition. **Meng-Si Zhu:** Investigation, Validation. **Mei-Lan Du:** Investigation. **Xu-Qin Ran:** Investigation. **Xiu-Ping Yan:** Writing – review & editing, Funding acquisition.

Declaration of Competing Interest

The authors declare that they have no known competing financial interests or personal relationships that could have appeared to influence the work reported in this paper.

Acknowledgements

This work was supported by the Guangdong Laboratory for Lingnan Modern Agriculture Project (NZ2021037), the National Natural Science Foundation of China (No. 22076066, 21804055 and 21775056), the Fundamental Research Funds for the Central Universities (No. JUSRP221002), the National First-class Discipline Program of Food Science and Technology (No. JUFSTR20180301), the Program of "Collaborative Innovation Center of Food Safety and Quality Control in Jiangsu Province".

Appendix A. Supporting information

Supplementary data associated with this article can be found in the online version at doi:10.1016/j.jhazmat.2021.128156.

References

Albatrni, H., Qiblawey, H., El-Naas, M.H., 2021. Comparative study between adsorption and membrane technologies for the removal of mercury. Sep. Purif. Technol. 257, 117833.
Chong, J.H., Sauer, M., Patrick, B.O., MacLachlan, M.J., 2003. Highly stable keto-enamine salicylideneanilines. Org. Lett. 5, 3823–3826.
Cui, W.-R., Jiang, W., Zhang, C.-R., Liang, R.-P., Liu, J., Qiu, J.-D., 2020. Regenerable carbohydrazide-linked fluorescent covalent organic frameworks for ultrasensitive detection and removal of mercury. ACS Sustain. Chem. Eng. 8, 445–451.
Cui, W.-R., Zhang, C.-R., Xu, R.-H., Chen, X.-R., Yan, R.-H., Jiang, W., Liang, R.-P., Qiu, J.-D., 2021. Low band gap benzoxazole-linked covalent organic frameworks for photo-enhanced targeted uranium recovery. Small 17, 2006882.
Cui, Y.Y., Ren, H.B., Yang, C.X., Yan, X.P., 2019. Facile synthesis of hydroxyl enriched microporous organic networks for enhanced adsorption and removal of tetrabromobisphenol A from aqueous solution. Chem. Eng. J. 373, 606–615.
Da, H.-J., Yang, C.-X., Qian, H.-L., Yan, X.-P., 2020. A knot-linker planarity control strategy for constructing highly crystalline cationic covalent organic frameworks: decoding the effect of crystallinity on adsorption performance. J. Mater. Chem. A 8, 12657–12664.
Ding, S.Y., Wang, W., 2013. Covalent organic frameworks (COFs): from design to applications. Chem. Soc. Rev. 42, 548–568.
Ding, S.Y., Dong, M., Wang, Y.W., Chen, Y.T., Wang, H.Z., Su, C.Y., Wang, W., 2016. Thioether-based fluorescent covalent organic framework for selective detection and facile removal of mercury(II). J. Am. Chem. Soc. 138, 3031–3037.
Frisch, M.J., et al., 2013. Gaussian 09, Revision E, p. 01.
Fryxell, G.E., Lin, Y., Fiskum, S., Birnbaum, J.C., Wu, H., Kemner, K., Kelly, S., 2005. Actinide sequestration using self-assembled monolayers on mesoporous supports. Environ. Sci. Technol. 39, 1324–1331.

Haase, F., Lotsch, B.V., 2020. Solving the COF trilemma: towards crystalline, stable and functional covalent organic frameworks. Chem. Soc. Rev. 49, 8469–8500.
Hsu-Kim, H., Kucharzyk, K.H., Zhang, T., Deshusses, M.A., 2013. Mechanisms regulating mercury bioavailability for methylating microorganisms in the aquatic environment: a critical review. Environ. Sci. Technol. 47, 2441–2456.
Huang, L., Shuai, Q., 2019. Facile approach to prepare sulfur-functionalized magnetic amide-linked organic polymers for enhanced Hg(II) removal from water. ACS Sustain. Chem. Eng. 7, 9957–9965.
Huang, L., Shen, R., Liu, R., Shuai, Q., 2020. Thiol-functionalized magnetic covalent organic frameworks by a cutting strategy for efficient removal of Hg^{2+} from water. J. Hazard. Mater. 392, 122320.
Huang, L., Liu, R., Yang, J., Shuai, Q., Yuliarto, B., Kaneti, Y.V., Yamauchi, Y., 2021. Nanoarchitectured porous organic polymers and their environmental applications for removal of toxic metal ions. Chem. Eng. J. 408, 127991.
Huang, N., Wang, P., Jiang, D., 2016. Covalent organic frameworks: a materials platform for structural and functional designs. Nat. Rev. Mater. 1, 16068.
Huang, N., Zhai, L., Xu, H., Jiang, D., 2017. Stable covalent organic frameworks for exceptional mercury removal from aqueous solutions. J. Am. Chem. Soc. 139, 2428–2434.
Huang, X., Cao, X., Wang, W., Zhong, H., Cao, Z., 2017. Preparation of a novel resin with acyl and thiourea groups and its properties for Cu(II) removal from aqueous solution. J. Environ. Manag. 204, 264–271.
Jiang, Y., Zhang, H., He, Q., Hu, Z., Chang, X., 2012. Selective solid-phase extraction of trace mercury (II) using a silica gel modified with diethylenetriamine and thiourea. Microchim. Acta 178, 421–428.
Kandambeth, S., Mallick, A., Lukose, B., Mane, M.V., Heine, T., Banerjee, R., 2012. Construction of crystalline 2D covalent organic frameworks with remarkable chemical (acid/base) stability via a combined reversible and irreversible route. J. Am. Chem. Soc. 134, 19524–19527.
Karak, S., Dey, K., Torris, A., Halder, A., Bera, S., Kanheerampockil, F., Banerjee, R., 2019. Inducing disorder in order: hierarchically porous covalent organic framework nanostructures for rapid removal of persistent organic pollutants. J. Am. Chem. Soc. 141, 7572–7581.
Linwei, H., Shengtang, L., Long, C., Xing, D., Jie, L., Mingxing, Z., Fuyin, M., Chao, Z., Zaixing, Y., Ruhong, Z., Zhifang, C., Shuao, W., 2019. Mechanism unravelling for ultrafast and selective $^{99}TcO_4^-$ uptake by a radiation-resistant cationic covalent organic framework: a combined radiological experiment and molecular dynamics simulation study. Chem. Sci. 10, 4293–4305.
Ma, H., Liu, B., Li, B., Zhang, L., Li, Y.-G., Tan, H.-Q., Zang, H.-Y., Zhu, G., 2016. Cationic covalent organic frameworks: a simple platform of anionic exchange for porosity tuning and proton conduction. J. Am. Chem. Soc. 138, 5897–5903.
McNutt, M., 2013. Mercury and health. Science 341, 1430.
Merí-Bofí, L., Royuela, S., Zamora, F., Ruiz-González, M.L., Segura, J.L., Muñoz-Olivas, R., Mancheño, M.J., 2017. Thiol grafted imine-based covalent organic frameworks for water remediation through selective removal of Hg(II). J. Mater. Chem. A 5, 17973–17981.
Merrifield, J.D., Davids, W.G., Macrae, J.D., Amirbahman, A., 2004. Uptake of mercury by thiol-grafted chitosan gel beads. Water Res. 38, 3132–3138.
Pearson, R.G., 1968. Hard and soft acids and bases, HSAB, part II: underlying theories. J. Chem. Educ. 45, 643.
Plazinski, W., Dziuba, J., Rudzinski, W., 2013. Modeling of sorption kinetics: the pseudo-second order equation and the sorbate intraparticle diffusivity. Adsorption 19, 1055–1064.
Qian, H.L., Meng, F.L., Yang, C.X., Yan, X.P., 2020. Irreversible amide-linked covalent organic framework for selective and ultrafast gold recovery. Angew. Chem. Int. Ed. 59, 17607–17613.
Rahman, Z., Singh, V.P., 2019. The relative impact of toxic heavy metals (THMs)(arsenic (As), cadmium (Cd), chromium (Cr)(VI), mercury (Hg), and lead (Pb)) on the total environment: an overview. Environ. Monit. Assess. 191, 1–21.
Segura, J.L., Mancheno, M.J., Zamora, F., 2016. Covalent organic frameworks based on Schiff-base chemistry: synthesis, properties and potential applications. Chem. Soc. Rev. 45, 5635–5671.
Sun, Q., Aguila, B., Perman, J., Earl, L.D., Abney, C.W., Cheng, Y., Wei, H., Nguyen, N., Wojtas, L., Ma, S., 2017. Postsynthetically modified covalent organic frameworks for efficient and effective mercury removal. J. Am. Chem. Soc. 139, 2786–2793.
Wu, X., Han, X., Liu, Y., Liu, Y., Cui, Y., 2018. Control interlayer stacking and chemical stability of two-dimensional covalent organic frameworks via steric tuning. J. Am. Chem. Soc. 140, 16124–16133.
Wu, X., Han, X., Xu, Q., Liu, Y., Yuan, C., Yang, S., Liu, Y., Jiang, J., Cui, Y., 2019. Chiral BINOL-based covalent organic frameworks for enantioselective sensing. J. Am. Chem. Soc. 141, 7081–7089.
Xu, H., Gao, J., Jiang, D., 2015. Stable, crystalline, porous, covalent organic frameworks as a platform for chiral organocatalysts. Nat. Chem. 7, 905–912.
Xu, R.-H., Cui, W.-R., Zhang, C.-R., Chen, X.-R., Jiang, W., Liang, R.-P., Qiu, J.-D., 2021. Vinylene-linked covalent organic frameworks with enhanced uranium adsorption through three synergistic mechanisms. Chem. Eng. J. 419, 129550.
Yoo, J., Cho, S.-J., Jung, G.Y., Kim, S.H., Choi, K.-H., Kim, J.-H., Lee, C.K., Kwak, S.K., Lee, S.-Y.J.Nl, 2016. COF-net on CNT-net as a molecularly designed, hierarchical porous chemical trap for polysulfides in lithium–sulfur batteries. Nano Lett. 16, 3292–3300.
Yu, J.-G., Yue, B.-Y., Wu, X.-W., Liu, Q., Jiao, F.-P., Jiang, X.-Y., Chen, X.-Q., 2016. Removal of mercury by adsorption: a review. Environ. Sci. Pollut. Res. 23, 5056–5076.
Yusran, Y., Fang, Q., Qiu, S., 2018. Postsynthetic covalent modification in covalent organic frameworks. Isr. J. Chem. 58, 971–984.
Zhang, Y., Li, H., Chang, J., Guan, X., Tang, L., Fang, Q., Valtchev, V., Yan, Y., Qiu, S., 2021. 3D Thioether-based covalent organic frameworks for selective and efficient mercury removal. Small 17, e2006112.
Zhao, C., Diercks, C.S., Zhu, C., Hanikel, N., Pei, X., Yaghi, O.M., 2018. Urea-linked covalent organic frameworks. J. Am. Chem. Soc. 140, 16438–16441.
Zhu, Y., Wan, S., Jin, Y., Wei, Z., 2015. Desymmetrized vertex design for the synthesis of covalent organic frameworks with periodically heterogeneous pore structures. J. Am. Chem. Soc. 137, 13772–13775.
Zou, Y., Wang, X., Khan, A., Wang, P., Liu, Y., Alsaedi, A., Hayat, T., Wang, X., 2016. Environmental remediation and application of nanoscale zero-valent iron and its composites for the removal of heavy metal ions: a review. Environ. Sci. Technol. 50, 7290–7304.